Peculiar many-body effects revealed in the spectroscopy of highly charged quantum dots

M. EDIGER[1], G. BESTER[2]*, A. BADOLATO[3], P. M. PETROFF[3], K. KARRAI[4], A. ZUNGER[2] AND R. J. WARBURTON[1]*

[1]School of Engineering and Physical Sciences, Heriot-Watt University, Edinburgh EH14 4AS, UK
[2]National Renewable Energy Laboratory, Golden, Colorado 80401, USA
[3]Materials Department, University of California, Santa Barbara, California 93106, USA
[4]Center for NanoScience and Department für Physik, Ludwig-Maximilians-Universität, 80539 München, Germany
*e-mail: G.Bester@fkf.mpg.de; R.J.Warburton@hw.ac.uk

Published online: 14 October 2007; doi:10.1038/nphys748

Coulomb interactions between electrons lead to the observed multiplet structure and breakdown of the Aufbau principle for atomic *d* and *f* shells[1]. Nevertheless, these effects can disappear in extended systems. For instance, the multiplet structure of atomic carbon is not a feature of graphite or diamond. A quantum dot is an extended system containing ∼10^6 atoms for which electron–electron interactions do survive and the interplay between the Coulomb energy, J, and the quantization energy, ΔE, is crucial to Coulomb blockade[2–5]. We have discovered consequences of Coulomb interactions in self-assembled quantum dots by interpreting experimental spectra with an atomistic calculation. The Coulomb effects, evident in the photon emission process, are tunable *in situ* by controlling the quantum dot charge from +6e to −6e. The same dot shows two regimes: $J \leq \Delta E$ for electron charging yet $J \simeq \Delta E$ for hole charging. We find a breakdown of the Aufbau principle for holes; clear proof of non-perturbative hole–hole interactions; promotion–demotion processes in the final state of the emission process, effects first predicted a decade ago[6]; and pronounced configuration hybridizations in the initial state. The level of charge control and the energy scales result in Coulomb effects with no obvious analogues in atomic physics.

We use InAs/GaAs dots (bound s, p and d orbitals) in tunnel contact with an electron reservoir that allows controlled charging[4,7]. Figure 1 shows optical charging of quantum dot A. There are abrupt changes in the photoluminescence at particular voltages signifying charging events. The charge in each plateau is known by identifying the singly charged exciton, X^{1-}, which has no fine structure[8] and a large extent in gate voltage, V_g (ref. 7). Figure 1 demonstrates charging in discrete steps from X^{6+} up to X^{6-}.

Underpinning the experiment is Coulomb blockade: the configuration of electrons with lowest energy is established by a tunnelling interaction with the electron reservoir[4,7]. For positive charging at large negative voltages, holes accumulate in the quantum dot from the optical excitation. At each voltage, a certain number of holes must accumulate before it becomes energetically favourable for an electron to tunnel into the dot from the Fermi sea, at which point recombination yields a photon. The number of holes required increases step-wise with increasing negative voltage. The transitions between the positively charged excitons are abrupt in voltage because the device does not rely on slow hole tunnelling[9], exploiting instead fast electron tunnelling.

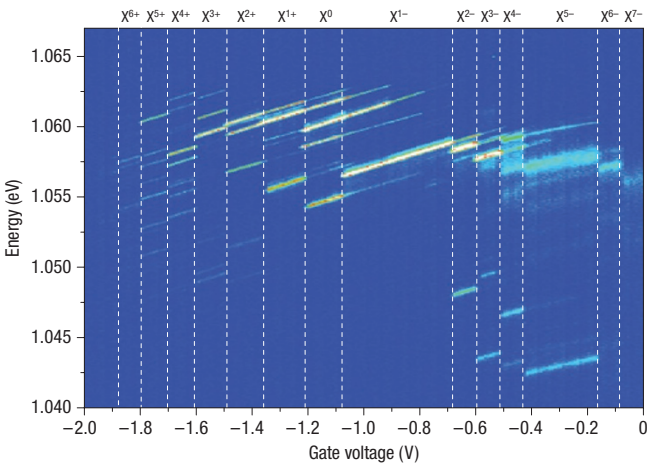

Figure 1 Charging diagram of single InAs/GaAs quantum dot A. Photoluminescence energy plotted against gate voltage, V_g. The photoluminescence intensity is represented with a colour scale, with blue (white) corresponding to 0 (2000) counts on the detector. The vertical lines mark the charging events.

We have calculated the optical properties of an InAs dot. In the single-particle step, the crystal potential is a superposition of atomic screened potentials v_α of atom type α at each relaxed atomic site $\mathbf{R}_{\alpha n}$, where n is the lattice site index: $V(\mathbf{r}) = \sum_{\alpha n} v_\alpha(\mathbf{r} - \mathbf{R}_{\alpha n})$. The pseudopotentials are adjusted so that the quasiparticle energies fit experimental data on bulk InAs and GaAs (ref. 10) thus representing valence electron correlations. The Schrödinger equation is solved in a basis set consisting of strained Bloch functions of the underlying bulk semiconductor[10]. This approach

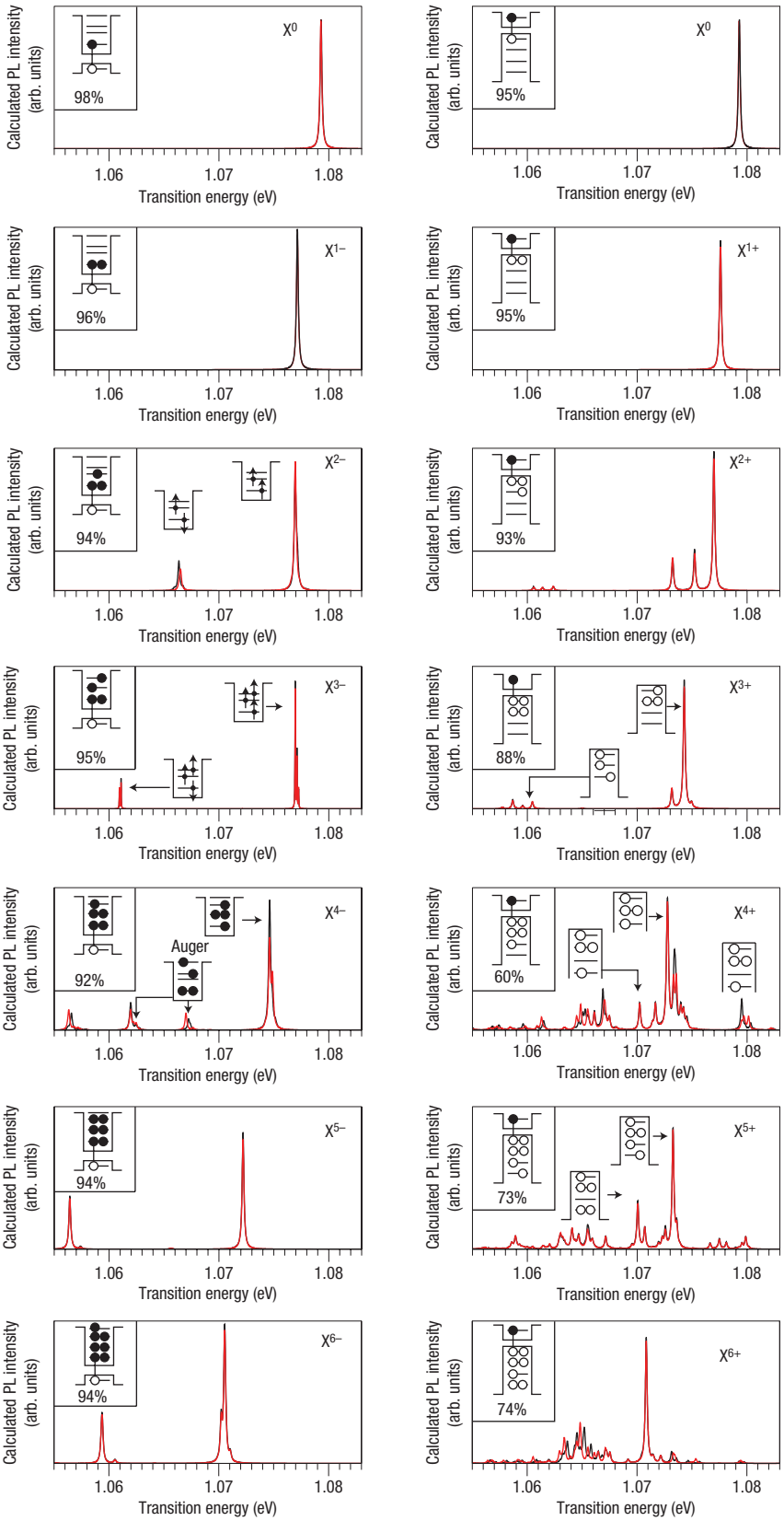

Figure 2 Calculated photoluminescence (PL) spectra for different exciton charges for the dot with circular base. The dot is a cylindrical InAs dot with 25 nm diameter and 2 nm height sitting on two monolayers of wetting layer. Red denotes [110] polarization, black [1$\bar{1}$0] polarization calculated for 5 K. The insets in the upper-left corner of each panel show the leading configuration of the initial states along with its weight in per cent. For some selected photoluminescence lines, the leading final-state configuration is shown.

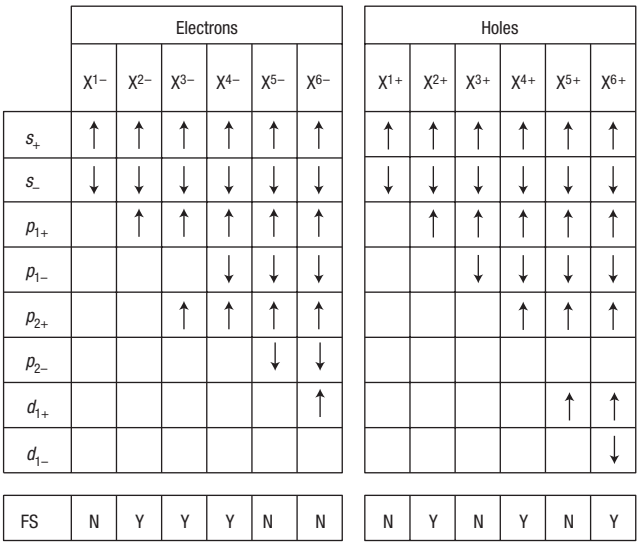

Figure 3 Calculated leading configurations for charged excitons. Left: one hole and N electrons; right: one electron and N holes. For the positively (negatively) charged states, the single electron (hole) in the initial state is in the lowest electron (hole) state. The last line indicates whether fine-structure effects are predicted (Y) or not (N).

captures the multiband, intervalley and spin–orbit interactions and also includes first- and second-order piezoelectric effects[11]. All of the valence single-particle levels of the dots are represented, for example, for an N-atom dot there are $2N$ occupied single-particle levels ($N \sim 10^6$). These levels have mixed angular momenta, mixed heavy hole–light hole and complex nodal structure, much like the states of a giant molecule containing a comparable number of atoms. This is different to effective-mass models[6,12] where the orbitals are hydrogenic-like. In the many-body step, we use a configuration interaction approach where all of the Slater determinants constructed from 12 electron and 12 hole single-particle states (counting spin) interact. The interaction consists of Coulomb and exchange integrals calculated from the atomistic single-particle wavefunctions. The screening function for these integrals is calculated following the microscopic model of Resta[13] and exhibits a smooth transition from unscreened at short range to screened at long range. This naturally includes both long- and short-range exchange[14]. Using atomistic orbitals to calculate many-particle interactions is different to most calculations of correlation in quantum nanostructures where the basis of single-particle states is taken from effective-mass models. That the inter-electronic integrals computed from effective-mass wavefunctions are very different to those computed from atomistic wavefunctions can be dramatically seen by the different ensuing symmetries of the charged exciton ground states[15]. Our method has provided a quantitative understanding of the unusual X^{2-} and X^{2+} fine structure[16].

Calculations for a cylindrical dot are shown in Fig. 2 where the dominant initial-state configuration is given for each charge state with its weight. The final-state configurations are shown for selected transitions. We interpret the experimental results with the model without fitting any of the nanostructure parameters. This approach is limited only by the imperfect knowledge of the real dots' morphology. The experiment does not measure directly the composition of the ground-state configuration. Nevertheless, information can be deduced on the basis of the sensitivity of the photoluminescence spectrum to the initial-state configuration, closed and open shells having very different optical signatures; and to the initial-state spin through fine structure, an electron–hole exchange interaction which leads to polarization-dependent energy splittings[8]. Only an unpaired hole (electron) in the positively (negatively) charged initial state leads to fine structure allowing an experimental discrimination between zero and finite spin. We find an excellent correspondence between our measured and calculated photoluminescence spectra, allowing us to uncover a number of physical effects.

(1) *Anomalous ground states*. We determine the ground-state configurations of charged excitons by minimizing the many-body energy as a function of the distribution of electrons and holes in the single-particle levels. Figure 3 shows that a system consisting of one hole and two, three, five, six, seven electrons and a system consisting of one electron and two, three, four, five holes follows the Aufbau principle whereas the others, X^{3-}, X^{5+} and X^{6+}, violate the Aufbau principle in that one low-energy level remains empty whereas a higher-energy level is filled. The calculations for X^{3-} predict an open-shell initial configuration (Fig. 2) that recombines into two final states split by 16 meV through electron–electron exchange. The initial state violates Aufbau in that the p_{1-} level remains empty whereas the higher-energy p_{2+} is filled: for dots of small height, the loss in single-particle energy on promoting $\varepsilon(p_{1-})$ to $\varepsilon(p_{2+})$ is more than compensated by the gain in exchange energy associated with forming a higher total spin[17]. Experimentally, the dot A X^{3-} photoluminescence is dominated by the open-shell lines split by 14 meV (Fig. 4), in excellent agreement with the theoretical prediction; the two closed-shell lines (green circles in Fig. 4) can be made out and arise from thermal occupation of the higher-energy initial state. Furthermore, the upper X^{3-} photoluminescence line has a clear fine structure, as predicted. For dot B (see Supplementary Information, Fig. S1), the open-shell and closed-shell X^{3-} lines have similar intensities—the two configurations are close to degenerate in this case; for dot C (see Supplementary Information, Fig. S2), the closed-shell X^{3-} photoluminescence lines dominate. These observations point to a slight decrease in rotational symmetry from dot A to B to C.

Theory predicts a very simple spectrum for X^{5-} that originates from a strongly dominant closed-shell initial configuration with no fine structure. In a calculated elongated dot, the lower X^{5-} peak weakens and a new lower-energy peak emerges (see Supplementary Information, Fig. S3). Experimentally, there is clear shell-filling for X^{5-}: dots A, B and C all have a large-V_g plateau extent and an absence of fine structure. Dot A shows one lower photoluminescence peak, consistent with the theory for the symmetric dot; dots B and C show two lower peaks, consistent with the theory for the elongated dot.

The open-shell ground state of X^{2+} predicted by the theory is confirmed by experiment. A polarization dependence in the transitions is found in both theory and experiment. Theoretically, X^{3+} has a closed-shell ground state with no polarization dependence in the photoluminescence. Likewise, the experimental photoluminescence has no measurable polarization dependence. In the experiment, the principal X^{3+} photoluminescence peak is slightly blue-shifted relative to the principal X^{2+} peak, closer to the theoretical prediction for the closed-shell X^{3+} (red-shift of 3 meV) than the open-shell X^{3+} (blue-shift of 6 meV). The lines in the experimental X^{3+} photoluminescence above the principal peak from dot A are not reproduced in the theory but these features are of lower relative intensity from dots B and C. The open-shell X^{4+} configuration with fine-structure splitting is confirmed experimentally through the strong polarization dependence of the transitions. X^{5+} has a most fascinating behaviour. In contrast to X^{5-}, X^{5+} is predicted to violate Aufbau in that the first d state is occupied before the second p state is filled. Furthermore, we

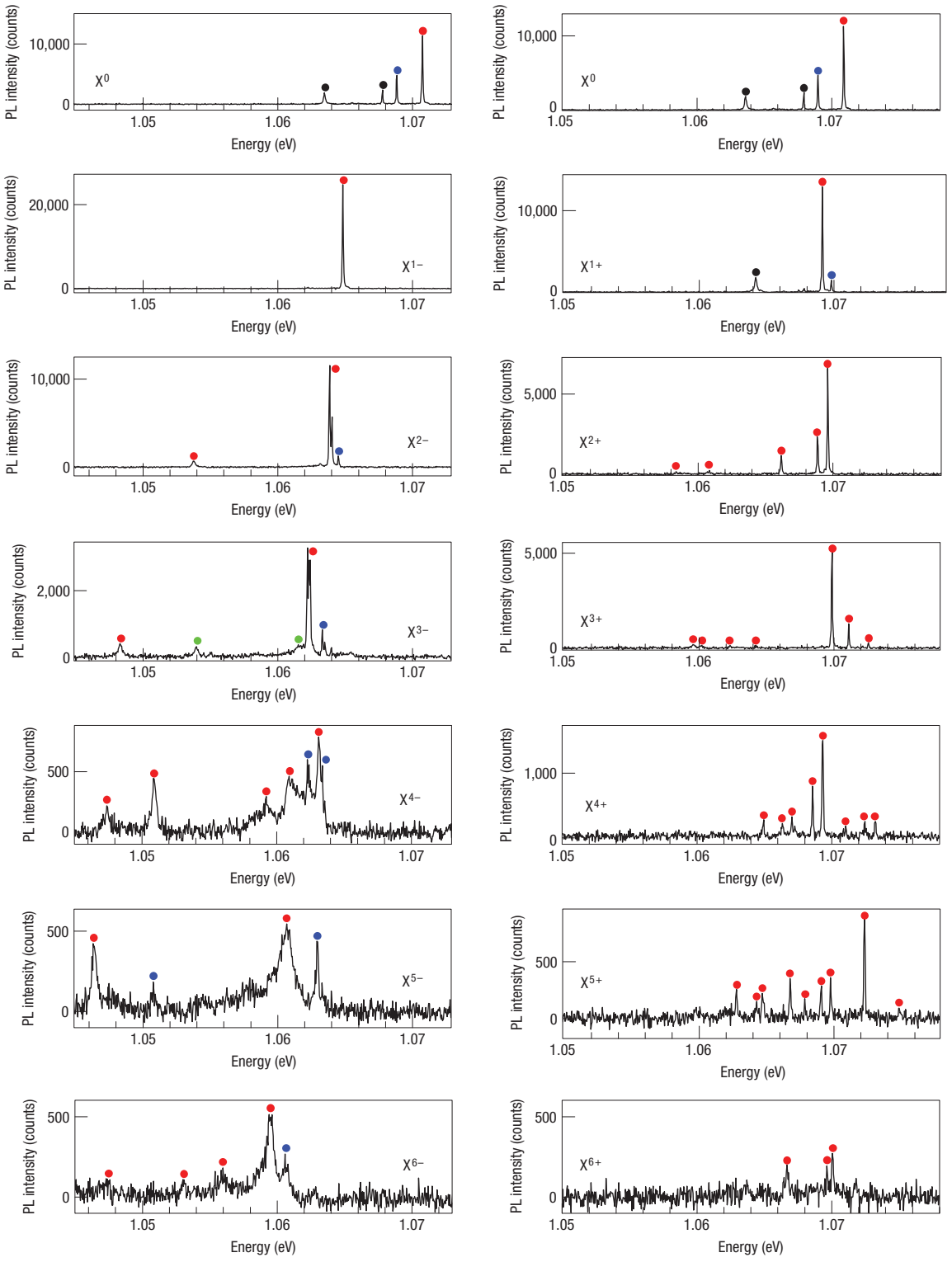

Figure 4 Measured photoluminescence spectra from dot A for different exciton charges. Photoluminescence intensity (840 s integration time) is plotted against energy for V_g corresponding to the centre of each charging plateau. Individual peaks are labelled: red circle denotes a photoluminescence peak from the particular exciton with charge n; blue circle emission from exciton with charge $n-1$; black circle biexciton-related emission; green circle emission from an excited initial-state configuration.

predict that the hole charging sequence is perturbed by the presence of the electron: without the electron, the second p state is not occupied at all[15]. Curiously, the predicted initial configuration is open shell, yet the photoluminescence is almost unpolarized, both in the experiment and in the theory, signifying a zero-spin-state coupling of the unpaired holes. Small fine-structure effects

are still present in the theoretical results, originating from the admixed (27%) configurations in the initial state; these effects are beyond the experimental resolution. Theoretically, the signature of the open-shell X^{5+} is the presence of a multitude of peaks with comparable intensity, whereas the closed-shell X^{5+} configuration has one strong peak accompanied by many very weak transitions. Experimentally, there are several strong photoluminescence lines, strongly supporting the open-shell configuration. The non-Aufbau filling of hole states continues for X^{6+} where p_2 is left half empty. A polarized experimental spectrum (dots A and B) with a few peaks agrees with the theoretical prediction but the X^{6+} photoluminescence is very weak.

(2) *Non-perturbative Coulomb interactions*. A perturbation treatment of the Coulomb interactions predicts a blue-shifted X^{1+} on the basis of a red-shifted X^{1-} (ref. 18). Indeed, our calculated Coulomb energies[17] $J_{hh} = 25.9\,\text{meV} > |J_{eh}| = 25.3\,\text{meV} > J_{ee} = 24.9\,\text{meV}$ lead to a $J_{hh} - J_{eh} = 0.6\,\text{meV}$ blue-shift of X^{1+} with respect to X^0. However, this effect is countered by the non-perturbative mixing of the $h_S^2 e_S^1$ configuration with other configurations, a mixing that produces an overall red-shift of X^{1+}, a clear feature in both experiment (Fig. 4) and theory (Fig. 2). This simple fact proves that hole–hole Coulomb interactions cannot be treated perturbatively.

(3) *Exchange-split final states*. In general, charged exciton states with an open-shell initial configuration decay into final states split by electron–electron or hole–hole exchange. For instance, X^{2-}, X^{3-}, X^{4-} and X^{6-} each have two photoluminescence lines arising from two possible final spin states, Fig. 2. The open-shell X^{2+} decays into three states, not two as for X^{2-}. The two holes in the X^{2+} final state are predominantly heavy hole in character and therefore follow the rules for spin-3/2 particles: there is a two-fold degenerate state with $J = 3$ and two singlets with $J = 0$ and $J = 2$. The X^{2+} initial state is split by the electron–hole exchange interaction and has total angular momentum $f = 2$ and $f = 1$ resulting in three transitions: $f = 1 \rightarrow J = 0$, $f = 1 \rightarrow J = 2$ and $f = 2 \rightarrow J = 3$. For all exciton charges, the exchange splittings in experiment and theory are in perfect correspondence with good quantitative agreement.

(4) *Correlation-induced 'promotion–demotion' exciton lines*. The X^{4-} photoluminescence consists of more than the two peaks expected from electron exchange. This observation heralds a new consequence of Coulomb interactions. When the number of carriers after recombination exceeds two, a final configuration can be generated by demoting one particle to a lower level (for example, p to s) and promoting another to a higher level (for example, p to d)[6,19]. These Auger-like configurations are themselves optically dark but admixture with bright configurations has a powerful effect on the photoluminescence spectrum. For X^{4-}, we find two further photoluminescence lines related to promotion–demotion where the electron d orbitals are occupied in the final states even though the d orbitals are empty in the initial state (Fig. 2). The original effective-mass model with parabolic confinement predicts six bright photoluminescence lines for X^{4-} (ref. 6) but this is artificially high owing to the high degeneracies in the single-particle states. Our calculations predict instead four X^{4-} bright lines. The inner two have significant promotion–demotion character and would not appear without the d shell. The energies of the innermost transitions depend on the symmetry—the two peaks move further apart in an elongated dot (see Supplementary Information, Fig. S3). In the experiment, Fig. 4 shows two weak peaks at low energy, a strong peak at high energy and two further peaks intermediate in energy with strange line shapes. Analysis of dots B and C reveals in each case three peaks at low energy again with some peculiar structure around the peak at high energy. Our conclusion is that the experiment matches the theory well but there are further peaks at high energy in the measured photoluminescence, arising perhaps from an excited initial-state configuration. X^{5-} has a closed initial shell and does not have exchange-split final states. Nevertheless, both the measured and calculated X^{5-} spectra exhibit a splitting into two dominant lines, a direct consequence of promotion–demotion. The large calculated mixing of Auger configurations in the final states (40% and 60% in the high and low peaks, respectively) gives rise to the large $\simeq$15 meV splitting of the two peaks. For the elongated dot, theory predicts that the lower-energy peak splits into two (see Supplementary Information, Fig. S3). This is exactly what we observe for dots B and C (see Supplementary Information, Figs S1, S2).

(5) *Configuration mixing in the initial states*. For the highly positively charged excitons, the likelihood of finding several symmetry-compatible many-body configurations is large. We obtain theoretically such a strong initial-state mixing especially for X^{4+} and X^{5+} where the majority configuration constitutes only 60% and 73%, respectively, of the initial state. The minority configurations open new recombination pathways (see also Supplementary Information, Fig. S4). Especially intriguing are photoluminescence transitions in both the experiment and the theory for X^{4+} and X^{5+} a few meV above the principal peak. An admixed configuration in the initial state with non-Aufbau character is responsible for these photoluminescence lines. For X^{4+}, it is the configuration where the fifth hole occupies the d and not the p_2 level. This opens pathways to a final configuration with an empty p_2 state, as shown in Fig. 2. Together with hole–hole exchange and promotion–demotion effects, this leads to very complex X^{4+} and X^{5+} photoluminescence spectra. The general feature of a principal line at high energy with a multitude of lines in a bandwidth of $\sim$10 meV is a feature in both experiment and theory. There is clearly a very strong dot dependence: in the theory, elongating the dot induces a considerable change to the X^{4+} and X^{5+} spectra. Similarly, dots A, B, C show marked differences for X^{4+} and X^{5+}. A more detailed understanding of X^{4+} and X^{5+} will probably be possible only with a more detailed picture of the real dot morphology.

METHODS

The quantum dots are self-assembled by molecular beam epitaxy and are separated by 17 nm of intrinsic GaAs from an n^+ GaAs layer. The dots are capped with 10 nm of undoped GaAs followed by a 105 nm AlAs/GaAs superlattice. Ohmic contacts are prepared to the back contact, the earth, after which a 5-nm-thick NiCr Schottky barrier is evaporated onto the sample surface. Voltage V_g is applied to the NiCr Schottky contact. Photoluminescence is excited non-resonantly at 850 nm, collected with a low-temperature confocal microscope (5 K) and detected with a spectrometer–InGaAs photodiode array set-up with a spectral resolution of 120 μeV.

Some photoluminescence lines extend in voltage beyond the host plateau. It is important to make an assignment of the photoluminescence lines to a particular exciton charge. We find that some photoluminescence lines extend beyond the plateau to more positive V_g but not to more negative V_g. (This is the consequence of a cascade: X^{n-} emission leaves behind n electrons, which then capture a hole and emit as $X^{(n-1)-}$ before the true ground-state configuration, X^{n-}, is re-established.) In addition, the photoluminescence intensity from a particular exciton decreases abruptly with increasing V_g once the exciton no longer forms the ground state. We can determine the V_g boundaries of each photoluminescence line to $\sim$10 mV, enabling us to assign each line to a particular charge without ambiguity, Fig. 4. In Fig. 1 there are some weak biexciton-related features but these can be spotted easily through their dependence on pump power.

Tunnelling does not shift the photoluminescence lines appreciably: even at the plateau edges, energy shifts in the photoluminescence through a tunnel hybridization cannot be made out in Fig. 1. However, the photoluminescence energies depend on the electric field, a Stark effect, and we find that the corresponding dipole moment and polarizability depend on charge, particularly for the positively charged excitons[9]. To facilitate comparison with

our theory, we extrapolate in Fig. 4 the photoluminescence spectra to zero electric field. This is crucial as it reveals a red-shifted X^{1+}, not a blue-shifted X^{1+} as a cursory inspection of Fig. 1 might suggest. None of the splittings in the experimental photoluminescence depend on electric field demonstrating the validity of this method.

Received 10 November 2006; accepted 12 September 2007; published 14 October 2007.

References

1. Goeppert Mayer, M. Rare-earth and transuranic elements. *Phys. Rev.* **60**, 184–187 (1941).
2. Yacoby, A., Heiblum, M., Mahalu, D. & Shtrikman, H. Coherence and phase sensitive measurements in a quantum dot. *Phys. Rev. Lett.* **74**, 4047–4050 (1995).
3. Tarucha, S., Austing, D. G., Tokura, Y., van der Wiel, W. G. & Kouwenhoven, L. P. Direct Coulomb and exchange interaction in artificial atoms. *Phys. Rev. Lett.* **84**, 2485–2488 (2000).
4. Miller, B. T. *et al.* Few-electron ground states of charge-tunable self-assembled quantum dots. *Phys. Rev. B* **56**, 6764–6769 (1997).
5. Reuter, D. *et al.* Coulomb-interaction-induced incomplete shell filling in the hole system of InAs quantum dots. *Phys. Rev. Lett.* **94**, 026808 (2005).
6. Wojs, A. & Hawrylak, P. Theory of photoluminescence from modulation-doped self-assembled quantum dots in a magnetic field. *Phys. Rev. B* **55**, 13066–13071 (1997).
7. Warburton, R. J. *et al.* Optical emission from a charge-tunable quantum ring. *Nature* **405**, 926–929 (2000).
8. Bayer, M. *et al.* Fine structure of neutral and charged excitons in self-assembled In(Ga)As/(Al)GaAs quantum dots. *Phys. Rev. B* **65**, 195315 (2002).
9. Finley, J. J. *et al.* Quantum-confined Stark shifts of charged exciton complexes in quantum dots. *Phys. Rev. B* **70**, 201308(R) (2004).
10. Wang, L.-W. & Zunger, A. Linear combination of bulk bands method for large-scale electronic structure calculations on strained nanostructures. *Phys. Rev. B* **59**, 15806–15818 (1999).
11. Bester, G., Wu, X., Vanderbilt, D. & Zunger, A. Importance of second-order piezoelectric effects in zinc-blende semiconductors. *Phys. Rev. Lett.* **96**, 187602 (2006).
12. Shumway, J., Franceschetti, A. & Zunger, A. Correlation versus mean-field contributions to excitons, multiexcitons, and charging energies in semiconductor quantum dots. *Phys. Rev. B* **63**, 155316 (2001).
13. Resta, R. Thomas–Fermi dielectric screening in semiconductors. *Phys. Rev. B* **16**, 2717–2722 (1977).
14. Franceschetti, A., Wang, L.-W., Fu, H. & Zunger, A. Short-range versus long-range electron–hole exchange interactions in semiconductor quantum dots. *Phys. Rev. B* **58**, R13367–R13370 (1998).
15. He, L., Bester, G. & Zunger, A. Electronic phase diagrams of carriers in self-assembled quantum dots: Violation of Hund's rule and the Aufbau principle for holes. *Phys. Rev. Lett.* **95**, 246804 (2005).
16. Ediger, M. *et al.* Fine structure of negatively and positively charged excitons in semiconductor quantum dots: Electron–hole asymmetry. *Phys. Rev. Lett.* **98**, 036808 (2007).
17. Bester, G. & Zunger, A. Compositional and size-dependent spectroscopic shifts in charged self-assembled $In_xGa_{1-x}As/GaAs$ quantum dots. *Phys. Rev. B* **68**, 073309 (2003).
18. Warburton, R. J. *et al.* Coulomb interactions in small charge-tunable quantum dots: A simple model. *Phys. Rev. B* **58**, 16221–16231 (1998).
19. Karrai, K. *et al.* Hybridization of electronic states in quantum dots through photon emission. *Nature* **427**, 135–138 (2004).

Acknowledgements

The work was supported by EPSRC (UK), US Department of Energy SC-BES under Contract No. DE-AC36-99GO10337 LAB-03-17, DAAD and SFB 631 (Germany) and SANDiE (EU). Correspondence and requests for materials should be addressed to R.J.W. or G.B. Supplementary Information accompanies this paper on www.nature.com/naturephysics.

Author contributions

M.E. carried out the experimental work under the supervision of R.J.W. and K.K; G.B. carried out the theoretical work in A.Z.'s group; A.B. fabricated the heterostructure in P.M.P.'s group. M.E., G.B., K.K., A.Z. and R.J.W. worked jointly on the interpretation of the results.